Control of ULF wave accessibility to the inner magnetosphere by the convection of plasma density

AGU PUBLICATIONS

JGR

Journal of Geophysical Research: Space Physics

RESEARCH ARTICLE
10.1002/2017JA024874

Special Section:
Dayside Magnetosphere Interaction

Key Points:
- ULF wave accessibility to the inner magnetosphere depends on plasmaspheric density structure generated during periods of strong convection
- A 3-D MHD model for ULF waves shows that eigenmodes are excited within plasmaspheric drainage plume density structures
- This provides a pathway for radiation belt energization by ULF waves at lower L shell than would otherwise be possible

Correspondence to:
A. W. Degeling,
degeling@sdu.edu.cn

Citation:
Degeling, A. W., Rae, I. J., Watt, C. E. J., Shi, Q. Q., Rankin, R., & Zong, Q.-G. (2018). Control of ULF wave accessibility to the inner magnetosphere by the convection of plasma density. *Journal of Geophysical Research: Space Physics*, *123*. https://doi.org/10.1002/2017JA024874

Received 17 OCT 2017
Accepted 2 JAN 2018
Accepted article online 10 JAN 2018

Control of ULF Wave Accessibility to the Inner Magnetosphere by the Convection of Plasma Density

A. W. Degeling[1], I. J. Rae[2], C. E. J. Watt[3], Q. Q. Shi[1], R. Rankin[4], and Q.-G. Zong[5]

[1]Institute of Space Science, Shandong University, Weihai, China, [2]Department of Space and Climate Physics, University College London, London, UK, [3]Department of Meteorology, University of Reading, Reading, UK, [4]Department of Physics, University of Alberta, Edmonton, Alberta, Canada, [5]Institute of Space Physics and Applied Technology, Peking University, Beijing, China

Abstract During periods of storm activity and enhanced convection, the plasma density in the afternoon sector of the magnetosphere is highly dynamic due to the development of plasmaspheric drainage plume (PDP) structure. This significantly affects the local Alfvén speed and alters the propagation of ULF waves launched from the magnetopause. Therefore, it can be expected that the accessibility of ULF wave power for radiation belt energization is sensitively dependent on the recent history of magnetospheric convection and the stage of development of the PDP. This is investigated using a 3-D model for ULF waves within the magnetosphere in which the plasma density distribution is evolved using an advection model for cold plasma, driven by a (VollandStern) convection electrostatic field (resulting in PDP structure). The wave model includes magnetic field day/night asymmetry and extends to a paraboloid dayside magnetopause, from which ULF waves are launched at various stages during the PDP development. We find that the plume structure significantly alters the field line resonance location, and the turning point for MHD fast waves, introducing strong asymmetry in the ULF wave distribution across the noon meridian. Moreover, the density enhancement within the PDP creates a waveguide or local cavity for MHD fast waves, such that eigenmodes formed allow the penetration of ULF wave power to much lower L within the plume than outside, providing an avenue for electron energization.

1. Introduction

One of the principal interests in ultralow frequency (ULF) waves within Earth's magnetosphere over the last several decades stems from their potential for interaction with high-energy radiation belt electrons (e.g., Elkington, 2006). ULF wave-particle interactions can lead to radially inward or outward electron transport, which in the former case results in energization through the conservation of the first adiabatic invariant M, (Degeling & Rankin, 2008; Fälthammar, 1965; Shprits et al., 2008), and in the latter case, loss to the magnetopause through magnetopause shadowing, (Degeling et al., 2013; Herrera et al., 2016; Turner et al., 2012). The mechanism by which the electrons and ULF waves interact, known as drift resonance, requires that the electron orbital motion, which is eastward due to the gradient-curvature drift in Earth's geomagnetic field, approximately matches the phase speed of the ULF waves (Elkington et al., 1999).

Ultralow frequency (ULF) magnetohydrodynamic (MHD) waves are commonly launched into the magnetosphere from the dayside magnetopause and propagate mainly in the antisunward direction (Allan & Poulter, 1992). The energy source of the waves is provided by oscillations of the magnetopause that can be caused by variations in the solar wind dynamic pressure (Claudepierre et al., 2009; Kepko & Spence, 2003; Kessel et al., 2004; Kim et al., 2002), shear flow (Kelvin-Helmholtz) instability along the morning and afternoon magnetopause flanks (Chen & Hasegawa, 1974; Mills et al., 1999; Rae et al., 2005; Walker, 1981), flux transfer events at the magnetopause (Gillis et al., 1987; Glassmeier et al., 1984; Russell & Elphic, 1978), or hot flow anomalies in the magnetosheath (Hwang & Sibeck, 2016). MHD Fast mode waves, which propagate across the magnetic field as compressional waves at the Alfvén speed $v_A = B/\sqrt{\mu_0 \rho}$ (where B and ρ are the magnetic field strength and plasma mass density, respectively), transmit wave power from the magnetopause into the magnetosphere interior. Both B and ρ are highly inhomogeneous within the magnetosphere: B is dominated by the geomagnetic field and varies roughly as L^{-3} in the equatorial plane (L is equatorial radius) within the inner

magnetosphere (Roederer, 1970); ρ also decreases with L in the equatorial plane within a region close to the Earth known as the plasmasphere (Dent et al., 2003; Denton et al., 2004) and can decrease abruptly at the edge of this region (known as the plasmapause) by 1 or 2 orders of magnitude, at about $L = 4$ or $5R_E$ (Dent et al., 2006). Both B and ρ generally have power law-type dependencies in the direction along the magnetic field. The resulting inhomogeneity in the Alfvén speed gives rise to strong the refraction and reflection of MHD Fast mode waves as they approach the inner magnetosphere (Allan & Poulter, 1992). Interference between the incident and reflected waves forms the so-called cavity resonance structure in the dayside magnetosphere (Piersanti et al., 2012; Walker, 1981), and waveguide modes propagating antisunward in the morning and afternoon flanks.

In contrast to the MHD Fast mode, the Shear Alfvén mode, which is characterized by a transverse field line displacement, propagates along the magnetic field (Hasegawa & Chen, 1974). These waves are reflected at the northern and southern ionospheric boundaries and form eigenmodes within the magnetosphere with natural frequencies that depend on the Alfvén speed distribution along the magnetic field, the local magnetic field line length (Samson et al., 1971), and ionospheric conductivity (Allan & Knox, 1979a). The polarizations of these eigenmodes have also been found to depend on the local magnetic topology (Kabin et al., 2007; Rankin et al., 2006). Linear mode conversion from MHD fast modes to Shear Alfvén eigenmodes occurs at locations within the magnetosphere where the MHD fast mode driver frequency matches the Shear Alfvén wave eigenfrequency, forming highly localized features known as field line resonances (FLRs) (Allan & Poulter, 1992; Rae et al., 2005; Walker, 2000). These have been used to determine the equatorial cold plasma density from ground-based observations (Dent et al., 2006; Vellante, Piersanti, Heilig, et al., 2014; Vellante, Piersanti, & Pietropaolo, 2014).

The plasmasphere (Denton et al., 2004) is formed by low-temperature plasma flowing along magnetic field lines from Earth's ionosphere. This plasma is trapped within Earth's magnetic field and has an azimuthal flow provided by Earth's rotational motion. As distance from the Earth increases, the plasma flow becomes increasingly affected by a sunward convective flow from the magnetotail, driven by magnetic reconnection in the magnetotail, and along the dayside magnetopause (Volland, 1973). In the dusk sector these flows are in opposition, and a stagnation point exists where the flows have equal strength. The streamline passing through this point marks the plasmapause boundary (Dent et al., 2003; Kale et al., 2007), separating trapped plasma flowing azimuthally around the Earth, and plasma that can escape to the magnetopause. The location of the plasmapause, being dependent on the rate of convection within the magnetosphere driven by day and nightside reconnection, is dynamic (Dent et al., 2006; Kale et al., 2009) and depends on the direction of the solar wind interplanetary magnetic field (IMF) since this strongly influences the rate and location of reconnection. A typical feature of geomagnetic storm activity is a switch in the IMF direction (O'Brien et al., 2001), and a corresponding increase in convection within the magnetosphere. The increased convection causes a sudden decrease in radius of the plasmapause location and results in the release of formerly trapped plasma from the plasmasphere along streamlines toward the dayside magnetopause (Carpenter & Lemaire, 1997; Dent et al., 2006). Finally, the escaping plasma forms a transient structure of density within the magnetosphere, known as a plasmaspheric drainage plume (PDP) (Sandel et al., 2003), which typically extends from a location around local dusk at roughly 5 R_E through the afternoon sector toward the dayside magnetopause and lasts for intervals on the order of a few days.

ULF wave propagation and mode conversion within the magnetosphere has been extensively modeled using magnetohydrodynamics (MHD) (Allan & Knox, 1979b; Allan & Poulter, 1992; Claudepierre et al., 2016; Degeling & Rankin, 2008; Degeling et al., 2011; Lee & Lysak, 1991; Lysak et al., 2015; Rankin et al., 2006; Singer et al., 1981; Waters et al., 2010), although only in the case of axisymmetric plasma density profiles. Given the importance of ULF waves for electron dynamics during storms (e.g., Degeling et al., 2014; Li et al., 2017; Mann & Ozeke, 2016; Tan et al., 2011; Zong et al., 2009), it is important to determine how azimuthal density structure within the magnetosphere can change the behavior of ULF wave properties during important geomagnetic events.

This paper reports an investigation of how a plasmaspheric drainage plume structure affects ULF wave propagation and accessibility to lower L shells in the afternoon sector of the magnetosphere and establishes whether this is important for the radial transport of electrons by ULF waves. These questions are addressed using a 3-D model for MHD waves in the magnetosphere with day/night asymmetry in the background magnetic field and a paraboloid magnetopause boundary. The cold plasma density is provided by a simple transport model driven by a Volland-Stern electrostatic potential (Volland, 1973). The importance of the plume

in the context of radiation belt dynamics is addressed by considering the ability of ULF waves to do work on electrons at successive stages during the plume development and comparing against the initial state where the plume is absent. This is done for a range of frequencies from 1 to 7 mHz. The rest of the paper is organized as follows: The next section gives an overview of the modeling components, including the background magnetic field in section 2.1, the ULF wave model in section 2.2, and the cold plasma density advection model in section 2.3. Results and discussion are presented in section 3, in which an example of the alteration of 4 mHz ULF wave mode structure during PDP evolution is examined (section 3.1), and the frequency dependence of ULF wave accessibility during PDP evolution is discussed (section 3.2). Our conclusions are presented in section 4.

2. Overview of the Numerical Models

Out full investigation incorporates a range of different models. ULF waves are modelled in a nonaxisymmetric 3-D magnetic field with a range of number density profiles that mimic the evolution of a plasmaspheric drainage plume. In this section, we describe each of the model components used in this investigation.

2.1. Background Magnetic Field and Coordinate System

A simple semianalytic model for a dipole-like magnetic field with day-night asymmetry and an enclosing dayside magnetopause boundary is the vacuum (i.e., curl free) magnetic field model of Stern (1985). In this model, a dipole field is situated within a conducting paraboloid shell that represents the magnetopause, where surface (Chapman-Ferraro) currents flowing along the shell cancel the magnetic field component normal to the surface, confining the magnetic flux. Inside the boundary the magnetic field may be described by $\mathbf{B}=\nabla\psi$, where ψ satisfies Laplace's equation with the boundary condition that $\nabla\psi\cdot\hat{\mathbf{n}}=0$ along the magnetopause, and $\hat{\mathbf{n}}$ is a unit vector perpendicular to this surface.

We use a curvilinear field-aligned coordinate system (α,β,γ), such that $\mathbf{B}=B_{oE}\nabla\alpha\times\nabla\beta$ (where $B_{oE}=-3.11\times10^{-4}$ T); γ is a coordinate aligned with the magnetic field (hence, $\gamma=\gamma(\psi)$), and Euler potentials α and β are constant along field lines. Using the covariant formalism described in D'haeseleer et al. (1991), a vector (say, $\mathbf{E}$) is described in terms of its covariant components and contravariant basis vectors ($\mathbf{e}^\alpha=\nabla\alpha$, $\mathbf{e}^\beta=\nabla\beta$ and $\mathbf{e}^\gamma=\nabla\gamma$) by $\mathbf{E}=E_\alpha\mathbf{e}^\alpha+E_\beta\mathbf{e}^\beta+E_\gamma\mathbf{e}^\gamma$. The metric coefficients $g^{ij}=\mathbf{e}^i\cdot\mathbf{e}^j$ characterize the geometric properties of the coordinate system. The Euler potentials α and β are defined numerically by field line tracing from starting locations in the equatorial plane to the northern and southern ionospheres, and the metric coefficients are obtained by centered finite differences.

2.2. ULF Waves

We model ULF waves throughout the magnetosphere by making a linear approximation following Rankin et al. (2006) and Degeling et al. (2010). Under ideal MHD conditions in a cold plasma, the equations for linear low-frequency waves are as follows:

$$\frac{\partial b}{\partial t}=-\nabla\times\mathbf{E} \tag{1}$$

$$\frac{1}{v_A^2}\frac{\partial\mathbf{E}}{\partial t}=\nabla_\perp\times\mathbf{b}-\frac{(\mu_0\mathbf{J}\times\mathbf{b})\times\mathbf{B}}{B^2}+\mu_0\mathbf{J}_{\text{ext}} \tag{2}$$

where $\mathbf{b}$ and $\mathbf{E}$ are the perturbed magnetic and electric fields, respectively, $\mathbf{B}$ and $\mu_0\mathbf{J}=\nabla\times\mathbf{B}$ are the ambient magnetic field and current density, respectively, and v_A is the Alfvén speed. The term $\mathbf{J}_{\text{ext}}$ is the external driver for exciting waves in the model and is only required at locations close to the magnetopause, elsewhere it is set to zero.

Under the restriction that $\mathbf{B}=B_{oE}\sigma\nabla\gamma$, (and hence $\mathbf{B}\cdot\mathbf{J}=0$ in our model geometry), it can be shown (Degeling et al., 2010) that

$$\left(\frac{1}{\sigma}G\cdot\begin{pmatrix}E'_\alpha\\E'_\beta\end{pmatrix}\right)'-\frac{\sqrt{g}}{v_A^2}G\cdot\begin{pmatrix}\ddot{E}_\alpha\\\ddot{E}_\beta\end{pmatrix}-\frac{1}{\sigma}\begin{pmatrix}-\partial/\partial\beta\left(\dot{b}_\gamma\sigma\right)\\\partial/\partial\alpha\left(\dot{b}_\gamma\sigma\right)\end{pmatrix}=\sqrt{g}\begin{pmatrix}\nabla\alpha\\\nabla\beta\end{pmatrix}\cdot\left(\mu_0\dot{\mathbf{J}}_{\text{ext}}\right) \tag{3}$$

where dashes and dots represent partial differentiation with respect to γ and t, respectively, $\sqrt{g}=(\nabla\alpha\times\nabla\beta\cdot\nabla\gamma)^{-1}$, and $\mathbf{G}$ is a 2×2 tensor given by

$$G=\begin{pmatrix}g^{\alpha\alpha}&g^{\alpha\beta}\\g^{\alpha\beta}&g^{\beta\beta}\end{pmatrix} \tag{4}$$

and $\dot{b}_\gamma$ is given in terms of the components of **E** by

$$\dot{b}_\gamma = -\sigma\left(\frac{\partial E_\beta}{\partial \alpha} - \frac{\partial E_\alpha}{\partial \beta}\right) \tag{5}$$

In Degeling et al. (2010), a spectral method for the β and γ directions was used to solve the above equations. However, for the present study we wish to evaluate the solution close to the parabolic magnetopause boundary and to account for arbitrary structures in the Alfvén speed, a task for which the finite element method (FEM) applied in the equatorial plane (as in the 2-D ULF wave model of Degeling et al., 2011) is more suitable. Therefore, we extend the model of Degeling et al. (2011) to 3D by using a spectral method for the γ direction only and 2-D FEM for the α and β directions to solve equations (3) and (5). The ULF wave electric field components are given by

$$\begin{pmatrix} E_\alpha \\ E_\beta \end{pmatrix} = \sum_{n=0}^{N} \begin{pmatrix} E_{\alpha n}(\alpha,\beta) \\ E_{\beta n}(\alpha,\beta) \end{pmatrix} \varphi_n(\hat{\gamma})\, e^{-i\omega t} \tag{6}$$

where ω is the wave frequency, $\varphi_n(\hat{\gamma})$ is a set of basis functions, and $\hat{\gamma} \in [-1, 1]$ is a scaled field-aligned coordinate (namely, $\hat{\gamma} = \gamma/\gamma_{\text{ion}}(\alpha,\beta)$, where $\gamma_{\text{ion}}(\alpha,\beta)$ is the value of γ at the ionosphere). For simplicity in the current model, the ionospheric Pederson conductance Σ_p is assumed to be much greater than the critical value $\Sigma_{pc} = 1/\mu_0 v_{Ai}$ (where v_{Ai} is the Alfvén speed at the ionosphere) (Allan & Knox, 1979a), such that nodes are assumed for the electric field at the ionosphere. This is enforced by choosing basis functions with $\varphi_n(\pm 1) = 0$ in the model, which are constructed using an orthogonal modification of Chebyshev polynomials.

ULF wave power dissipation in the ionosphere due to finite conductance is included phenomenologically by introducing a small imaginary part to the driver frequency $\omega \to \omega + i\nu$, where $2\nu/\omega = 1 - \left(\left(\Sigma_p - \Sigma_{pc}/\right)/\left(\Sigma_p + \Sigma_{pc}\right)\right)^2$ (Degeling et al., 2010) (this can be obtained by considering the ionospheric reflection coefficient for the wave electric field Scholer, 1970).

Further information on the details of the spectral method used in the model are given in Appendix A.

2.3. Cold Plasma Transport Model

The cold plasma density ρ is governed by its continuity equation: $\partial\rho/\partial t + \nabla\cdot(\rho\mathbf{u}) = S - L$. Here the plasma flow $\mathbf{u} = (-\nabla\Phi \times \mathbf{B})/B^2$ (due to an assumed electrostatic potential Φ) is synonymous with the motion of magnetic flux under ideal MHD conditions, and S and L are plasma source and loss terms, respectively. Under ideal MHD conditions it is assumed that plasma transport along magnetic field lines occurs very rapidly in order to remove field-aligned potential gradients, and this field-aligned transport is instantaneous in our model. Hence, any variations in $S - L$ occurring at the ionosphere are effectively dispersed over the entire field line. Since $\mathbf{B} \parallel \nabla\gamma$ in our model, $\mathbf{u}\cdot\nabla\gamma = \mathbf{0}$, and the continuity equation in the covariant formalism becomes

$$\frac{\partial}{\partial t}\left(\sqrt{g}\rho\right) + \frac{\partial}{\partial \alpha}\left((\mathbf{u}\cdot\nabla\alpha)\sqrt{g}\rho\right) + \frac{\partial}{\partial \beta}\left((\mathbf{u}\cdot\nabla\beta)\sqrt{g}\rho\right) = S - L \tag{7}$$

In the special case that $S - L = 0$, the product $\left(\sqrt{g}\rho\right)$ is a function of α, β, and t only; hence, it can be shown from the definition of $\sqrt{g}$ that on a given field line $\rho = \rho_0(\alpha,\beta,t)\left(B/B_0\right)^2$, where the subscript "0" indicates equatorial values. For example, for a dipole field this approximately gives $\rho \approx \rho_0(\alpha,\beta,t)\left(r/r_0\right)^{-6}$.

We will therefore assume that the effective field-aligned profile for $S - L$ varies as $\left(r/r_0\right)^{-Q}$, where Q is a constant, and $0 \le Q \le 6$. We therefore have a quasi-2-D model, in which the plasma density is given by $\rho \approx \rho_0(\alpha,\beta,t)\left(r/r_0\right)^{Q-6}$. This functional form is supported by observations and often used in empirical models, whereby field-aligned variations are fit to any value between r^0 and r^{-6} (Denton et al., 2004). The equatorial density $\rho_0(\alpha,\beta,t)$ is then given by solving equation (7) with the right-hand side set to zero. This is carried out by calculating marker particle trajectories for the plasma density in the equatorial plane and interpolating ρ_0 from the markers onto a fixed equatorial mesh at each output time step, following the method of Nunn (1993).

The electric field used to drive the convective flow **u** is assumed to be electrostatic, with model potential Φ in accordance with Volland (1973) and (Stern, 1975) given by

$$\Phi = \Phi_0 L^k \sin(\phi) - \frac{\Omega_E B_{0E} R_E^2}{L} \tag{8}$$

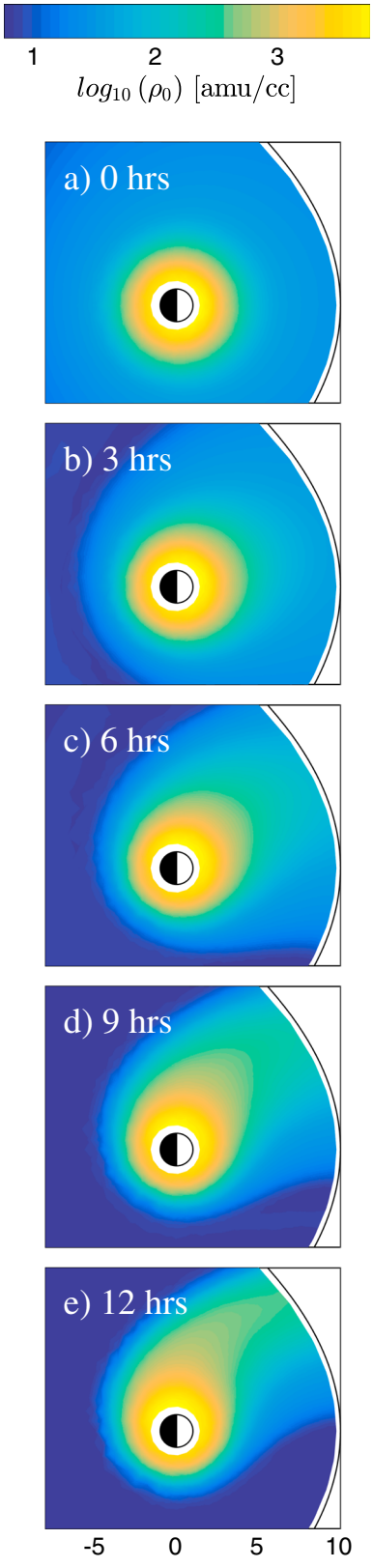

Figure 1. Equatorial density profiles at various stages during the development of the plasmaspheric density plume, under the action of the Volland-Stern electrostatic potential (equation 8, with $E_0 = 0.25$ mV/m and $k = 1$).

where the amplitude Φ_0 sets the convection electric field strength, Ω_E denotes the Earth's angular rotation frequency, L and ϕ are the L shell parameter and azimuthal angle (with zero at local midnight) in the equatorial plane, respectively, and k is set to 1 for a constant dawn-dusk convection electric field.

The initial equatorial mass density profile is given by $\log(\rho_0) = (1-w)\log\left(\rho_1 (L/L_1)^{q_1}\right) + w\log\left(\rho_2 (L/L_2)^{q_2}\right)$. The terms on the right-hand side represent plasmasphere and plasmatrough density profiles, respectively. To provide a smooth transition between plasmasphere densities and plasmatrough densities, w is chosen to be a function of L that equals zero for $L \leq L_1$ and one for $L \geq L_2$ and varies smoothly from zero to one in-between.

An initial profile with an eroded plasmapause is chosen with parameters $(L_1, L_2) = (3, 6)$, $(q_1, q_2) = (-4, -1)$ and $(\rho_1, \rho_2) = (600, 30)$ amu/cm^3, respectively. In this paper, our aim is to show how changes in density structure in the magnetosphere can change the properties and behavior of ULF waves driven by magnetopause oscillations. Future work will determine the sensitivity of ULF wave behavior to variations in the initial plasma density profile.

For the purposes of this paper, a simplistic scenario is considered, in which the above initially symmetric plasma profile is assumed to change with time (t) as a result of an applied dawn-dusk convection electric field. The density profile at $T = 0$ is set as above (consistent with $\Phi_0 = 0$); then Φ_0 is set to a constant value of 1.59 keV for $T > 0$ (corresponding to a dawn-dusk convection electric field strength of 0.25 mV/m). The resulting evolution in equatorial mass density is given in Figure 1. This figure shows the textbook development of a plume structure in the afternoon sector (e.g., Goldstein & Sandel, 2005) as plasma flows along streamlines toward the magnetopause. A sharp plasmapause boundary also develops as low-density plasma flows sunward into the morning sector from the nightside (e.g., Goldstein et al., 2005). Both of these effects impact the accessibility of ULF wave power to the inner magnetosphere, as demonstrated in the next section.

3. Results and Discussion

All of the ULF wave results in this paper are generated using the same spatial amplitude profile and direction for the ULF wave source vector $\mathbf{J}_{\text{ext}}$. The amplitude is an approximate Gaussian function of distance along the magnetopause, centered at 12 magnetic local time (MLT), with a half width of ~18 R_E. The direction of $\mathbf{J}_{\text{ext}}$ is set parallel to the magnetopause, such that the resulting force $\mathbf{J}_{\text{ext}} \times \mathbf{B}_0$ is perpendicular to the boundary.

We wish to characterize the effect of the evolving plasma density profile on the distribution of ULF wave power within the magnetosphere. Using the models detailed above, we examine the wave behavior in a series of density profiles taken at hourly intervals from the density model (some examples are shown in Figure 1). We assume that the time scales of wave propagation through the closed magnetosphere are small compared to an hour (Chi et al., 2006) and so at every hour during the formation of the plasmaspheric drainage plume, we consider these density profiles to be a temporally constant profile. We then calculate the spatial distribution of ULF waves that result from a continuously driven source with constant amplitude and single frequency. In so doing, the wave equations (equation (3)) reduce to elliptic PDEs with $\partial^2/\partial t^2$ replaced by $-\omega^2$. The pertinent input

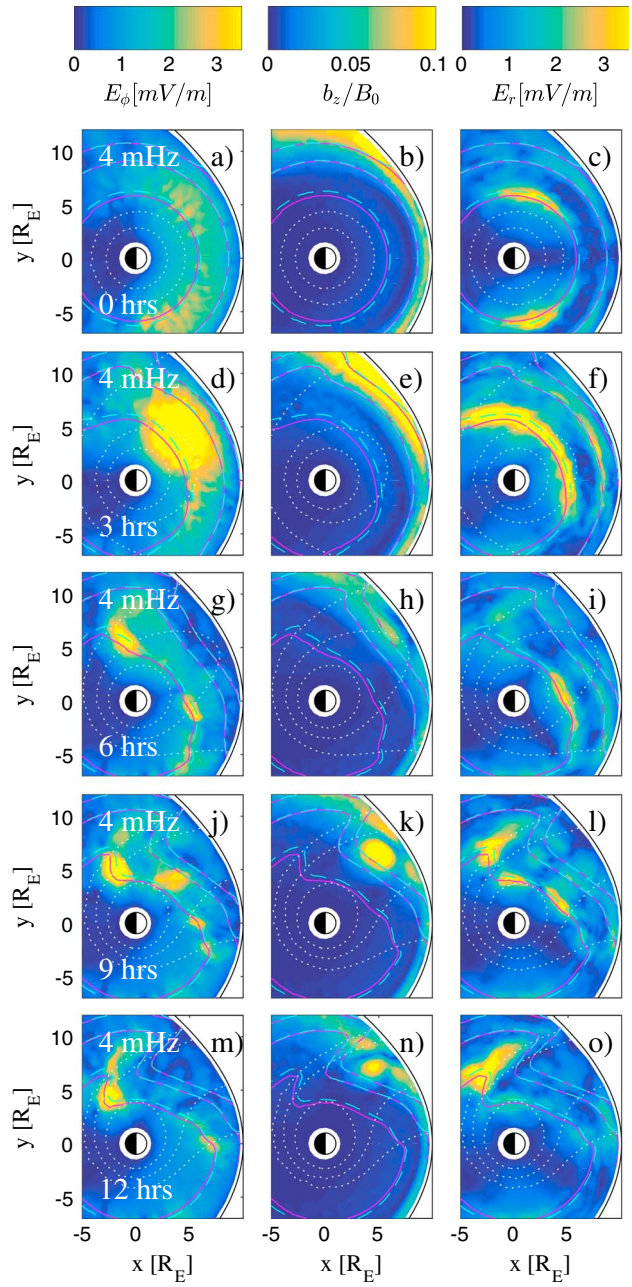

Figure 2. Equatorial maps of ULF wave components E_ϕ, b_z/B_0 and E_r, for 4 mHz ULF waves, at various stages during the development of the plasmaspheric density plume shown in Figure 1.

parameters for this study are therefore the ULF wave driver frequency ω, and the elapsed time in hours t after the convection field is initiated.

3.1. Alteration of ULF Wave Mode Structure During PDP Evolution

We first focus on the ULF wave characteristics for a set of models with constant driving frequency $f = 4$ mHz but varying number density models that mimic the behavior of a plasmaspheric drainage plume. Figure 2 shows example 2-D profiles in the equatorial plane of the ULF wave amplitude (components E_r, E_ϕ, and b_z/B_0) resulting from a continuously driven 4 mHz source along the magnetopause, for the stages of plume development shown in Figure 1 (corresponding to elapsed times of 0, 3, 6, 9, and 12 h, respectively). In each plot, white dotted contours indicate plasma density at 10, 100, and 1,000 amu/cm^3, respectively. Also, plotted in each figure are the locations of resonant surfaces for the lowest order Shear Alfvén Wave (SAW) eigenmodes, for driven excitations at 4 mHz (solid magenta and dashed cyan contours, for the "toroidal" and "poloidal" SAW polarizations, respectively). It is important to note, however, that designations of poloidal and toroidal waves can become misleading for SAWs in compressed-dipole magnetic fields, as demonstrated in Kabin et al. (2007). Only the locations for eigenmodes with even north-south symmetry are shown in Figure 2 (i.e., with an antinode in **E** at the equator) as these are the only available modes given the north-south symmetry in both the geometry and driver used in this model.

Figures 2a–2c (at $t = 0$ h) show a typical example of the excitation of fundamental mode field line resonances (FLRs) at an equatorial radius of about 6 R_E in the morning and afternoon sectors, due to resonant coupling from MHD fast mode waves launched from the magnetopause. This example shows clear symmetry about the noon/midnight meridian, as expected from the corresponding symmetries in the ULF wave source and the Alfvén speed profile. These FLRs are similar in structure to those seen in previous models (e.g., Claudepierre et al., 2016; Degeling et al., 2010, 2011) with axisymmetric density structure.

Figures 2d–2f (at $t = 3$ h), taken after the plasma density profile has developed a bulge toward the magnetopause in the afternoon sector, show a dramatically altered radiation pattern. The increased density along the dayside and particularly in the afternoon sector has shifted the resonant surfaces significantly earthward, allowing a deeper penetration of low m (azimuthal mode number) MHD fast mode waves into the afternoon sector. These waves form a broad peak in E_ϕ centered at roughly $(r, \phi) = (6R_E, 15\text{MLT})$ and a corresponding peak in b_z/B_0 at higher L. These fast mode waves have a much greater amplitude than found at $t = 0$ h using the same driver at the magnetopause. Associated with the localized fast modes is a strongly excited toroidal-mode FLR (visible in E_r, peaked near local dusk) along the fundamental SAW resonant surface that stretches from the late morning sector across the dayside into the evening sector.

Figures 2g–2i, 2j–2l, and 2m–2o, corresponding to $t = 6$, 9, and 12 h, respectively, show an interesting progression in ULF wave activity as the plasma density bulge in the afternoon sector extends further toward the magnetopause and narrows into a drainage plume.

We first concentrate on wave activity within the plasmaspheric drainage plume, before discussing interesting wave behavior on the duskward gradient of the plume. The strongly excited MHD fast mode and FLR in the afternoon sector evident at 3 h has largely disappeared by $t = 6$ h, with ULF wave activity reduced to a similar level found at $t = 0$ h, albeit at lower L shell. By $t = 9$ h, however, a localized peak in E_ϕ and b_z/B_0 has reappeared, at $L = 5$ and 7, respectively, and 15 MLT. This corresponds with approximately the central axis of the plume structure. Associated FLRs along the fundamental mode resonant surface are visible in E_r in the

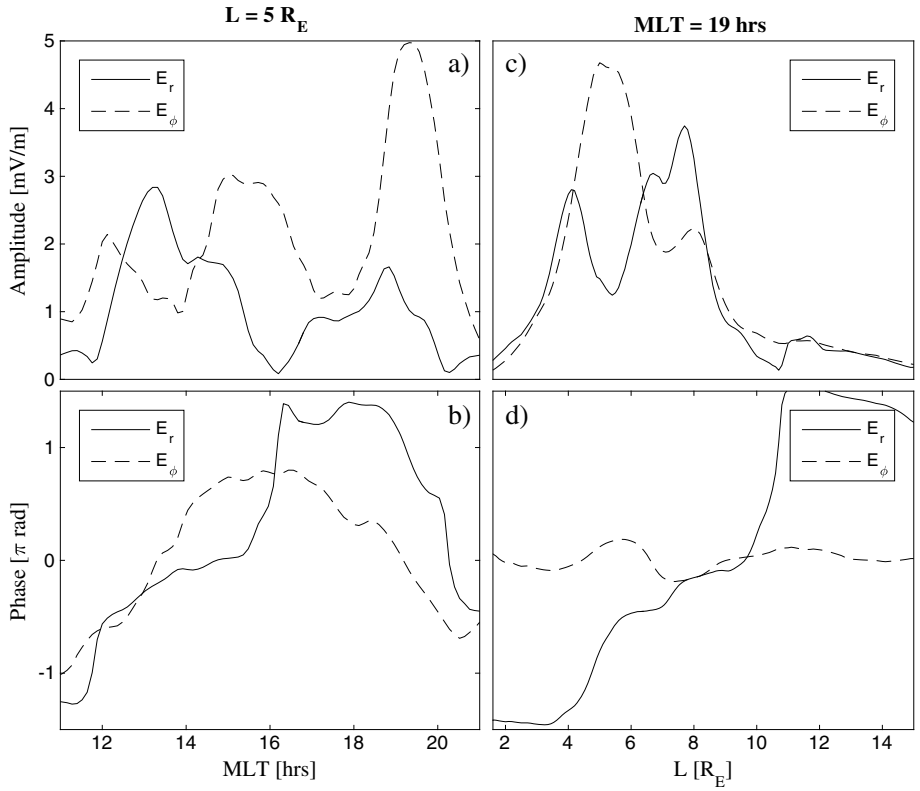

Figure 3. Equatorial maps of ULF wave components E_r, E_ϕ and b_z/B_0 for 4 mHz ULF waves, at various stages during the development of the plasmaspheric density plume shown in Figure 1.

afternoon sector, centered at (*L*,MLT) (4,18) and (4.5,14), respectively. Weaker peaks in E_r also appear close to the higher harmonic resonant surfaces within the density plume. These peaks appear to be centered on the sunward and duskward flanks of the plume and are separated in MLT by a minimum along the plume axis.

Observations of ground-based ULF wave power in and around a plasmaspheric drainage plume (Abe et al., 2006) indicate that near $L = 5.5$, the ULF wave power inside the plume appeared weaker than the power outside the plume. Figure 2 indicates that the relationship between power inside and outside of the plume is significantly more complicated and depends upon frequency, radial distance, and stage of evolution in the plume.

As the density plume evolves from $t = 6$ to 12 h, the fundamental mode SAW resonant surfaces develop a kink in the postdusk sector, which in turn becomes a "zigzag" (i.e., a multivalued function of MLT), along the duskward fringe of the density plume. It is interesting that a localized peak in E_ϕ develops where the resonant surface becomes approximately radially aligned, and strongly peaked structures in E_r are also found nearby at higher L, where the resonant surface narrows to a cusp. To examine the mode structure for the $f_d = 4$ mHz, $t = 9$ h case (plot 2k) , the components E_r and E_ϕ are interpolated along an arc from 11 to 21 MLT at a fixed *L* of 5 R_E (i.e., an MLT baseline), and along a radius from *L* of 2 to 10, at a fixed MLT of 19 h (i.e., a radial baseline), and shown in Figure 3. The top row of plots in the figure show the amplitude variation as a function of MLT and *L* in the left- and right-hand columns, respectively, whereas the bottom row of plots shows the phase variation in the same format.

The MLT baseline at 5 R_E shown in Figures 3a and 3b passes through plasmaspheric density plume in the afternoon sector, indicating the mode structure in this region. There are three strong peaks in E_ϕ occurring at approximately 12, 15, and 19 h MLT, respectively, and two main peaks in E_r at 13 and 19 MLT, with nodes (accompanied by π rad phase changes) at 12, 16, and 20 MLT. The phase is approximately stationary across the peaks in E_r and the central peak in E_ϕ, indicating they are antinodes. In other words, the ULF waves appear to have formed an eigenmode structure within the PDP, with E_ϕ and E_r components having odd and even parity modes across the plume, respectively.

The peak in E_ϕ at roughly 15 MLT coincides with a region of roughly constant phase, whereas the peaks at 12 and 19 MLT are both associated with significant changes in phase with MLT (corresponding to approximately π rad for the stronger peak at 19 MLT). Given that the MLT baseline intersects the fundamental SAW resonant surfaces at both 12 and 19 MLT, it is natural to expect FLRs to form. However, it is expected that externally driven FLRs would exhibit a peak in E_r and π rad phase change in the radial direction. For the FLRs appearing in this situation, the roles of r and ϕ seem reversed. We note that the direction of the gradient in the local Alfvén continuum has changed dramatically due to the evolution of magnetospheric plasma density. As noted earlier, Figure 2 shows that the resonant surface has an approximately radial alignment at 19 MLT (and a minor kink at 12 MLT appears to provide a local radial alignment in the resonant surface at this location also), indicating that the local gradient in Alfvén continuum is in the azimuthal direction, not the radial direction. Hence, during the evolution of the plasmaspheric drainage plume, the change in direction of the gradient of the Alfvén continuum can lead to atypical FLR behavior.

The radial baseline at 19 h MLT also passes through peaks in E_r at $L \approx 4\ R_E$ and $L \approx 7–8\ R_E$ close to the cusp in the SAW resonant surface. The phase plot in Figure 3d shows that the amplitude peak at $L \approx 4\ R_E$ is associated with a phase shift of π radians, indicating an FLR; however, the phase change is not large for the higher L case.

3.2. Frequency Dependence of ULF Wave Accessibility During PDP Evolution

We have seen above that ULF waves at $f = 4$ mHz have significantly greater access to the inner magnetosphere in the presence of a plasmaspheric drainage plume, with localized regions of enhanced wave amplitudes within and duskward of the density maximum. The next natural step is to investigate whether wave accessibility is a function of frequency. To simplify this analysis, we have developed a method to combine the important contributions of different ULF wave perturbations into a single parameter that indicates the potential for drift-resonant interactions with radiation belt electrons.

We consider the rate of work done by the waves on equatorially mirroring particles. The rate of work is given by $dW/dt = q\mathbf{E} \cdot \mathbf{v}_d + (M/\gamma)\,\partial B/\partial t$, where M is the magnetic moment, γ is the relativistic correction factor, and $\mathbf{v}_d$ is the drift velocity of a particle (of charge q), given by $\mathbf{v}_d = (\mathbf{E} \times \mathbf{B} + (M/q\gamma)\,\mathbf{B} \times \nabla B)\,/B^2$. Inserting the expression for $\mathbf{v}_d$ into the rate of work done gives $dW/dt = (M/\gamma)\,dB/dt$, where dB/dt (to first order for ease of calculation, indicated by B_1) is given by

$$\frac{dB_1}{dt} = \frac{\mathbf{E} \times \mathbf{B}_0 \cdot \nabla B_0}{B_0^2} + \frac{\partial b_z}{\partial t} \tag{9}$$

Equation (9) provides an estimate of the total rate of change of magnetic field strength B at a given location. The first term estimates the rate of change of magnetic field strength due to the advection of gradients in B at the "field line velocity" $\mathbf{v}_{fl} = \mathbf{E} \times \mathbf{B}_0/B_0^2$. The second term gives the rate of change of magnetic field strength due to explicit local changes in B, for example, due to $\nabla \cdot \mathbf{v}_{fl}$ characteristic of MHD fast mode waves.

We therefore adopt dB_1/dt evaluated in the equatorial plane as a metric for the distribution of ULF wave activity available for electron energization and investigate how this varies with changes in the driver frequency f_D and elapsed time as the plasma density distribution evolves. To this end, a series of calculations were performed with frequency steps of 0.5 mHz from 1 to 7 mHz and with hourly steps in time through the density model from 0 to 24 h. A selection from these parameter scans are shown in Figure 4 to summarize our results. These plots show the equatorial distribution of $|dB_1/dt|$ at frequencies of 2.5, 4.0, 5.5, and 7.0 mHz (first to fourth columns), and time steps of 3 h from 0 to 12 h (first to fifth rows, similar to previous figures). White dotted lines in these figures again indicate plasma density contours, the magenta dashed lines indicate surfaces of constant L^* (levels 3,5,7 and 9), where $L^* = (B_{0E}/B)^{1/3}$.

The light colored regions of these plots illustrate zones within the magnetosphere where significant wave power is available for particle energization compared to the initial conditions displayed in the top row. The location of these regions varies dramatically with both frequency and the elapsed time. First, comparing the results at 4 mHz (Column 2; plots b, f, j, n and r) with Figure 2, the combination of peaks in E_ϕ and b_z together provide a peak in $|dB_1/dt|$ in the afternoon sector, occurring at $t \approx 3$ h and again at $t \approx 9$ h from $L^* \approx 4$ to 7. Similar peaks in the afternoon sector occur at $t \approx 6$ h at 5.5 and 7 mHz, and between 9 and 12 h at 2.5 mHz.

Another interesting feature in these plots is that a peak in $|dB_1/dt|$ appears in the late morning sector, at $t \approx 3$ and 6 h for the 5.5 and 7 mHz cases (plots 4g, h, k and l). To examine whether these peaks may be significant

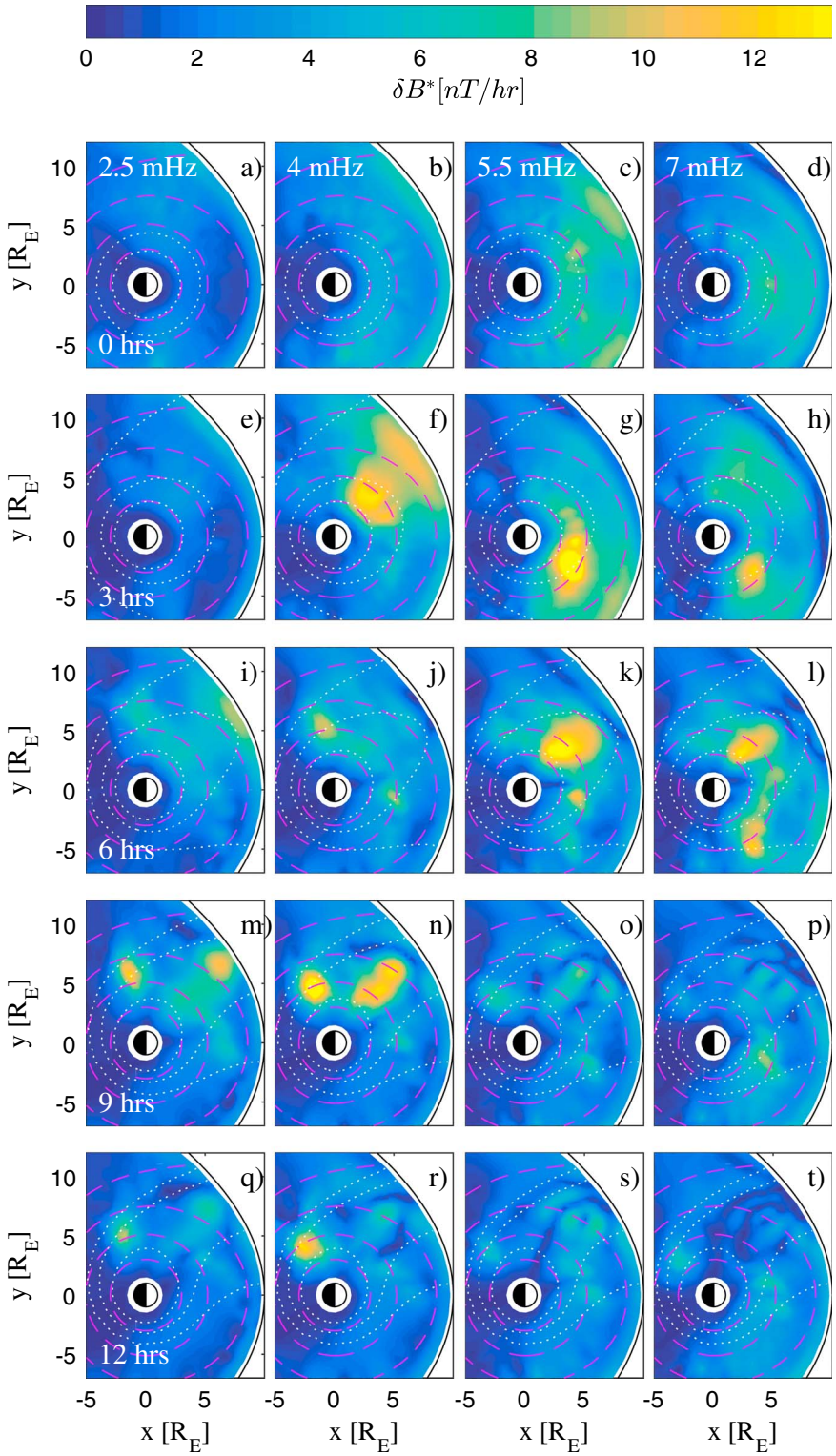

Figure 4. Equatorial maps of $|dB_1/dt|$ for driver frequencies of 2.5, 4, 5.5, and 7 mHz (columns), at various stages during the development of the plasmaspheric density plume shown in Figure 2 (rows).

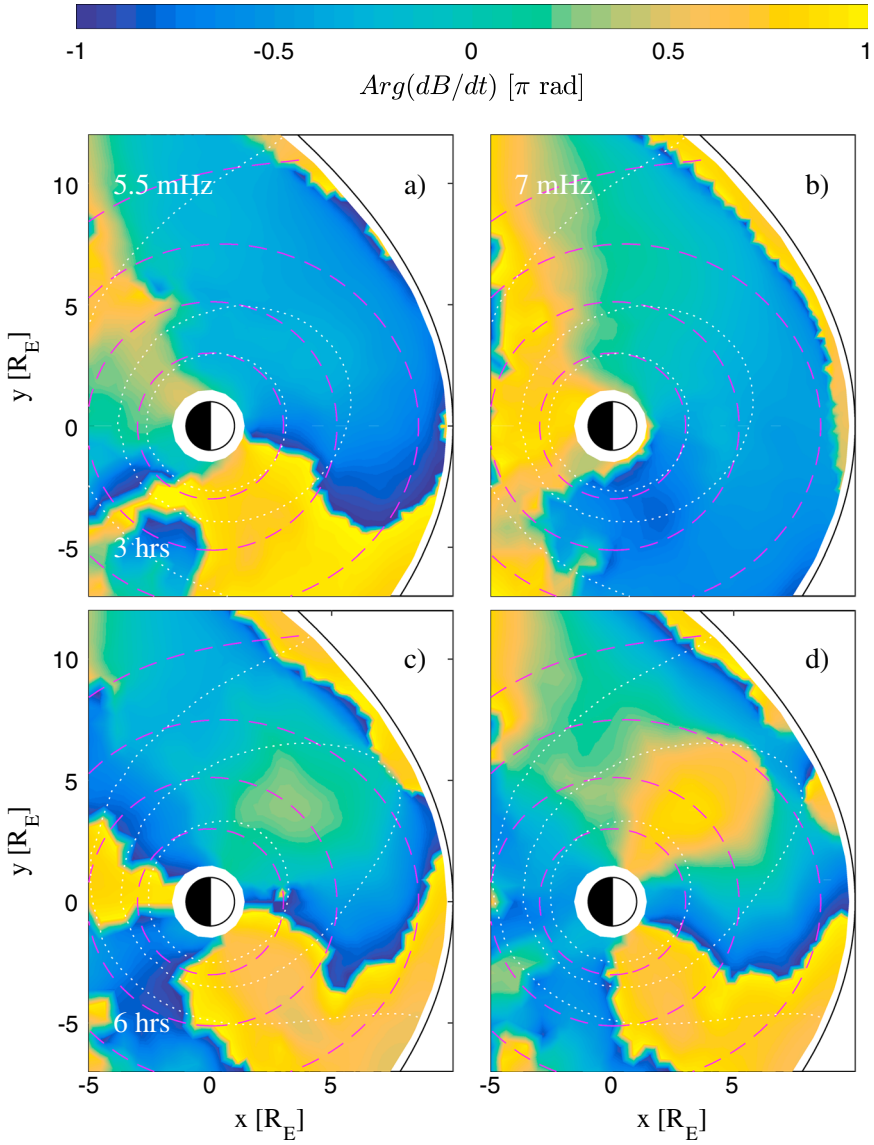

Figure 5. Equatorial maps of the phase of dB_1/dt for the cases of 5.5 and 7 mHz (columns) after elapsed times of 3 h and 6 h (rows).

for electron energization, equatorial maps of the phase of dB_1/dt are shown in Figure 5 for these cases. These figures indicate that the phase increases azimuthally from approximately 9 MLT across the dayside magnetosphere for both cases at $t \approx 3$ h (top row) and from 9 MLT to 16 MLT at $t \approx 6$ h (bottom row). Since the phase gradient is directed eastward, these waves are able to interact resonantly with electrons whose drift velocity matches the local wave phase velocity. The eastward ULF wave propagation across the dayside may be explained by considering surfaces of constant phase launched simultaneously along the magnetopause (as is the case for this simulation). These surfaces propagate more slowly into the magnetosphere in the afternoon sector where the Alfvén speed is lower due to increased density. Therefore, the resulting phase fronts refract eastward from the morning sector as long as the convection of plasma maintains a corresponding gradient in density and Alfvén speed. The results shown in Figures 2 and 4 indicate that ULF wave coupling to the inner magnetosphere is a sensitive function of the plasma density distribution and driver frequency. In particular, peaks in power injection (from the same ULF source distribution along the magnetopause) appear to coincide with the establishment of eigenmodes in the afternoon sector that correspond and evolve with the plasma density profile.

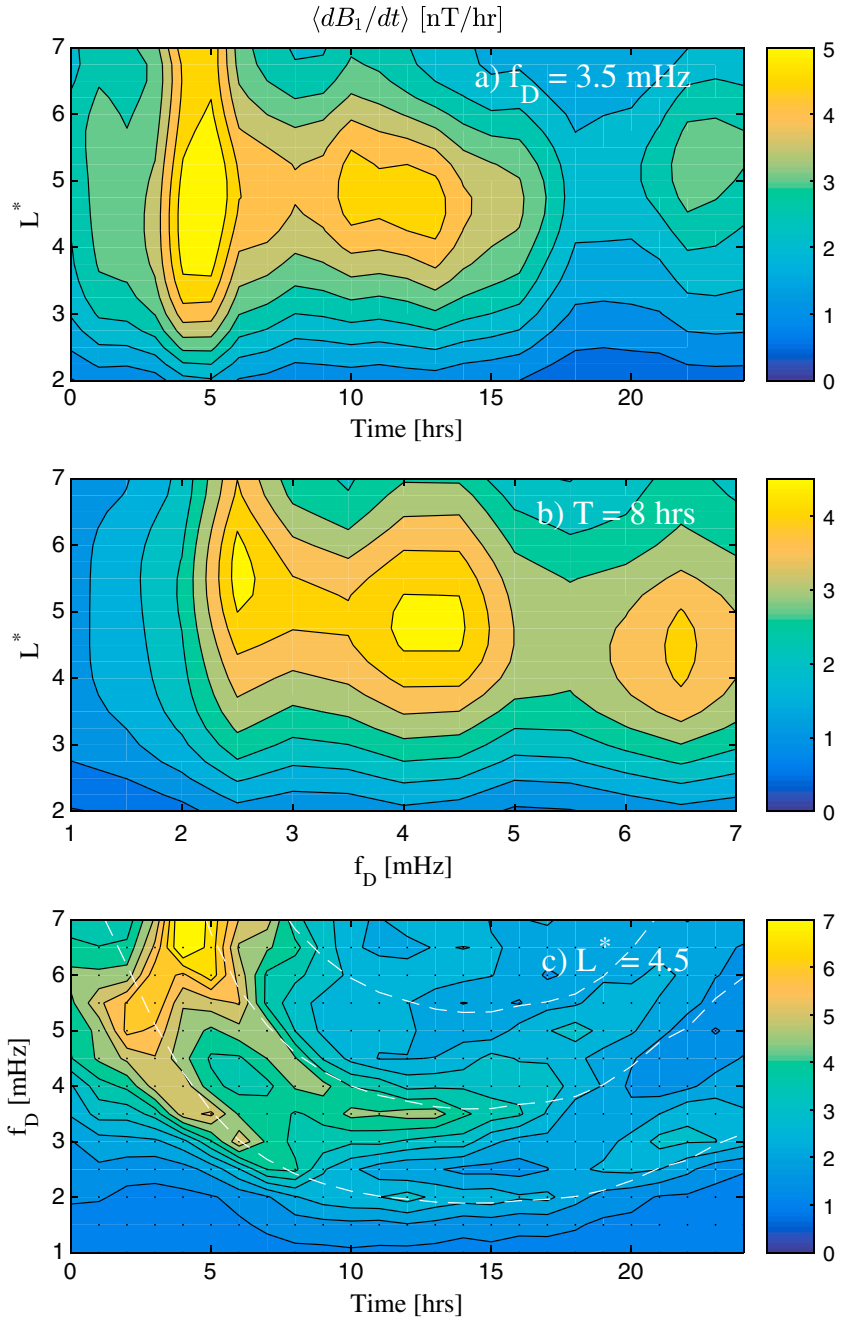

Figure 6. Contour plots of the $\langle dB_1/dt \rangle$ data set, showing variations as a function of: a) t and L^*, holding f_D constant at 3.5 mHz; b) f_D and L^*, holding t constant at 8 h; and c) t and f_D, holding L^* constant at 4.5 (Black dots indicate data point locations).

An overall indicator of the availability of ULF wave power for electron energization at a given L^* is provided by calculating the expectation value of dB_1/dt, given by

$$\left\langle \frac{dB_1}{dt} \right\rangle = \frac{1}{2\pi} \left(\oint_{L^*} \left| \frac{dB_1}{dt} \right|^2 d\phi \right)^{1/2} \tag{10}$$

The integrand in this expression is interpolated along a series of constant L^* contours (for $2 \leq L^* \leq 7$) to calculate $\langle dB_1/dt \rangle$ for each of the model runs comprising the parameter scans in both f_D and elapsed time t. Figures 6a and 6b show the variation of $\langle dB_1/dt \rangle$ with L^* as a function of t (holding f_D fixed at 3.5 mHz) and f_D

(holding t fixed at 8 h), respectively, while Figure 6c shows the variation of $\langle dB_1/dt \rangle$ with f_D as a function of t (holding L^* fixed at 4.5).

Figure 6a clearly shows that the availability of ULF wave power at a given frequency is peaked at particular time intervals, corresponding to the excitation of trapped modes within the evolving plasma density distribution. The amplitude of peaks in $\langle dB_1/dt \rangle$ is shown to decrease with time. This is because the extent of the trapped modes in MLT reduces with t as the PDP structure narrows and also because the coupling efficiency to the modes appears to decrease with time. This figure also shows that at 3.5 mHz, the amount of power available in the range $4 \leq L^* \leq 5$ is higher than the initial value over the first 16 h as the PDP develops and that it is roughly a factor of 2 higher for $4\ \text{h} \leq T \leq 12\ \text{h}$.

Figure 6b shows significant peaks in $\langle dB_1/dt \rangle$, which at $t = 8$ h, occur at 2.5, 4–4.5, and 6.5 mHz, at L^* values of 5.5, 5.0, and 4.5 respectively. Keeping in mind that the waves are excited by the same amplitude driver regardless of their frequency, this figure indicates the resonant excitation of the trapped modes. It also suggests that the PDP configuration at a given time will have a filtering effect on a broadband ULF wave source at the magnetopause. Peaks in $\langle dB_1/dt \rangle$ are at progressively lower L shells for increasing frequency as is expected from a more simple plasma density model — long field lines at high L support lower resonant frequencies than short field lines at low L.

Figure 6c shows how the frequency dependence of $\langle dB_1/dt \rangle$ varies with time at $L^* = 4.5$. This plot shows that the peaks shown in Figures 6a and 6b are intersections through a family of eigenfrequencies that have a clear time dependence as the PDP structure evolves. A simple model for the eigenfrequencies is given by considering a simplified dispersion relation for MHD fast mode waves in the equatorial plane of the magnetosphere: $\omega^2 = \omega_{\|}^2 + \left(k_L^2 + (m/L)^2\right) v_A^2$, where $\omega_{\|}$is the eigenfrequency for oscillations along field lines (taken to be the lowest SAW eigenfrequency here), and k_L is a radial wave number. The turning point for MHD fast mode waves is given by setting k_L to zero. A resonance may be expected if the azimuthal mode number m at the turning point matches an integer number of half-wavelengths (N) across the width of the plasma density plume, that is, $m = N\pi/\Delta\phi$, where $\Delta\phi$ is the azimuthal width of the plume. Hence, the trapped mode eigenfrequencies may be estimated by $\omega_N \approx \left(\omega_{\|}^2 + (N\pi/L\Delta\phi)^2 v_A^2\right)^{1/2}$. The values of $\omega_{\|}$ and v_A are evaluated as a function of the elapsed time t from the ULF wave model data by finding their minimum values along a line of constant L which passes through the plume. The values of $\Delta\phi$ and L are adjustable parameters in this simple model and are set to $\pi/3$ and 6.3, respectively, to give the white dashed lines shown in Figure 6c, for $N = 1$, 2, and 3. These curves follow a trend that is dominated by the variation of the minimum Alfvén speed with time, which decreases with time as the plasmaspheric density plume forms and then begins to increase with time as the plume density gradually empties to the magnetopause. The curves appear to agree fairly well with the peaks in $\langle dB_1/dt \rangle$ from the ULF wave model for $N = 1$ and 2 for the first 15 h, and the curve for $N = 3$ appears to coincide with a possible peak at high frequency for times between 6 and 9 h (and is visible in Figure 6b at 6.5 mHz), although this peak diminishes rapidly with time. For later times ($t > 15$ h), the peaks for $N = 1$ and 2 show an increasing trend at a rate that is more rapid than predicted by the simple model. This is most probably due to the fact that the plume width in MLT is gradually decreasing with time, whereas a constant value for $\Delta\phi$ is used in the model.

4. Conclusion

Using a 3-D MHD model for ULF waves, we have demonstrated how the development of a plasmaspheric drainage plume affects the accessibility of dayside ULF wave power to radiation belt electrons. By performing a series of numerical experiments over a range of driver frequencies from 1 to 7 mHz, the distribution of ULF waves was mapped at successive stages in the evolution of a PDP structure. Clear evidence was found of the establishment of trapped MHD fast mode waves within the PDP, enabling the penetration of ULF waves to lower L shell, and excitation of higher amplitudes by a cavity resonance. A metric for the ability of ULF waves to do work on the electrons is used to indicate zones and conditions where coupling between the ULF wave and electrons is potentially significant. These results underline the importance of the recent history of the plasmasphere and magnetospheric convection in providing a state in which the radiation belts are susceptible to interactions with ULF waves driven by magnetopause perturbations.

Appendix A: Further Details on the Wave Model

Rather than using a set of Shear Alfvén Wave eigenfunctions for the basis functions in the spectral method (as used in Degeling et al., 2010), a more standard approach (Galerkin's method using modified Chebyshev

polynomials Boyd, 2000) is taken here. This requires that the field-aligned coordinate be scaled to the interval $[-1, 1]$, namely, $\hat{\gamma} = \gamma / \gamma_{\text{ion}}(\alpha, \beta)$, where $\gamma_{\text{ion}}(\alpha, \beta)$ is the value of γ at the ionosphere. The partial differentials in equations (3) and (5) are transformed such that $\frac{\partial}{\partial \gamma} \rightarrow \left(\frac{\partial \hat{\gamma}}{\partial \gamma}\right) \frac{\partial}{\partial \hat{\gamma}}$ and $\frac{\partial}{\partial \alpha}|_{\gamma} \rightarrow \frac{\partial}{\partial \alpha}|_{\hat{\gamma}} + \left(\frac{\partial \hat{\gamma}}{\partial \alpha}\right) \frac{\partial}{\partial \hat{\gamma}}$ (and similarly for $\frac{\partial}{\partial \beta}$).

The basis functions are $\varphi_n(x) = \left(1 - x^2\right) U_n(x)$ (where $U_n(x)$ is type-2 Chebyshev polynomials), which satisfy the orthogonality condition $\int_{-1}^{1} w(x) \varphi_n \varphi_k dx = \pi/2 \delta_{nk}$ with weight $w(x) = \left(1 - x^2\right)^{-1/2}$. This is a convenient choice because $\varphi'(x) = -(n+1)\left(1 - x^2\right)^{-1/2} T_n(x)$ (where $Tn(x)$ is type-1 Chebyshev polynomials), with orthogonality condition $\int_{-1}^{1} w^{-1}(x) \varphi'_n \varphi'_k dx = \pi/2 (n+1)^2 \delta_{nk}$.

Acknowledgments

This work is supported by the National Natural Science Foundation of China (41774172 and 41574157). C. E. J. W. is supported by STFC (ST/M000885/1) and NERC (NE/P017274/1). R. Rankin acknowledges support by the Canadian Space Agency. The model output data (and a Matlab function for producing the figures in this article) are publicly available at http://doi.org/10.5285/7d2cc962-d4cf-4ce6-b3ae-96bc825c977a.

References

Abe, S., Kawano, H., Goldstein, J., Ohtani, S., Solovyev, S. I., Baishev, D. G., & Yumoto, K. (2006). Simultaneous identification of a plasmaspheric plume by a ground magnetometer pair and IMAGE Extreme Ultraviolet Imager. *Journal of Geophysical Research*, *111*, A11202. https://doi.org/10.1029/2006JA011653

Allan, W., & Knox, F. (1979a). Dipole field model for axisymmetric Alfven waves with finite ionosphere conductivities. *Planetary and Space Science*, *27*(1), 79–85.

Allan, W., & Knox, F. (1979b). Effect of finite ionosphere conductivities on axisymmetric toroidal Alfven wave resonances. *Planetary and Space Science*, *27*(7), 939–950.

Allan, W., & Poulter, F. (1992). ULF waves-their relationship to the structure of the Earth's magnetosphere. *Reports on Progress in Physics*, *55*, 533–598.

Boyd, J. P. (2000). *Chebyshev and Fourier spectral methods* (2nd ed.). New York: Dover.

Carpenter, D., & Lemaire, J. (1997). Erosion and recovery of the plasmasphere in the plasmapause region. *Space Science Reviews*, *80*, 153–179. https://doi.org/10.1023/A:1004981919827

Chen, L., & Hasegawa, A. (1974). A theory of long-period magnetic pulsations: 1. Steady state excitation of field line resonance. *Journal of Geophysical Research*, *79*(7), 1024–1032. https://doi.org/10.1029/JA079i007p01024

Chi, P. J., Lee, D.-H., & Russell, C. T. (2006). Tamao travel time of sudden impulses and its relationship to ionospheric convection vortices. *Journal of Geophysical Research*, *111*, A08205. https://doi.org/10.1029/2005JA011578

Claudepierre, S. G., Toffoletto, F. R., & Wiltberger, M. (2016). Global MHD modeling of resonant ULF waves: Simulations with and without a plasmasphere. *Journal of Geophysical Research: Space Physics*, *121*, 227–244. https://doi.org/10.1002/2015JA022048

Claudepierre, S. G., Wiltberger, M., Elkington, S. R., Lotko, W., & Hudson, M. K. (2009). Magnetospheric cavity modes driven by solar wind dynamic pressure fluctuations. *Geophysical Research Letters*, *36*, L13101. https://doi.org/10.1029/2009GL039045

Degeling, A. W., & Rankin, R. (2008). Resonant drift echoes in electron phase space density produced by dayside Pc5 waves following a geomagnetic storm. *Journal of Geophysical Research*, *113*, A10220. https://doi.org/10.1029/2008JA013254

Degeling, A. W., Rankin, R., & Elkington, S. R. (2011). Convective and diffusive ULF wave driven radiation belt electron transport. *Journal of Geophysical Research*, *116*, A12217. https://doi.org/10.1029/2011JA016896

Degeling, A. W., Rankin, R., Kabin, K., Rae, I. J., & Fenrich, F. R. (2010). Modeling ULF waves in a compressed dipole magnetic field. *Journal of Geophysical Research*, *115*, A10212. https://doi.org/10.1029/2010JA015410

Degeling, A. W., Rankin, R., Murphy, K., & Rae, I. J. (2013). Magnetospheric convection and magnetopause shadowing effects in ULF wave-driven energetic electron transport. *Journal of Geophysical Research: Space Physics*, *118*, 2919–2927. https://doi.org/10.1002/jgra.50219

Degeling, A. W., Rankin, R., & Zong, Q.-G. (2014). Modeling radiation belt electron acceleration by ULF fast mode waves, launched by solar wind dynamic pressure fluctuations. *Journal of Geophysical Research: Space Physics*, *119*, 8916–8928. https://doi.org/10.1002/2013JA019672

Dent, Z., Mann, I., Goldstein, J., Menk, F., & Ozeke, L. (2006). Plasmaspheric depletion, refilling, and plasmapause dynamics: A coordinated ground-based and IMAGE satellite study. *Journal of Geophysical Research*, *111*, A03205. https://doi.org/10.1029/2005JA011046

Dent, Z., Mann, I., Menk, F., Goldstein, J., Wilford, C., Clilverd, M., & Ozeke, L. (2003). A coordinated ground-based and IMAGE satellite study of quiet-time plasmaspheric density profiles. *Geophysical Research Letters*, *30*(12), 1600. https://doi.org/10.1029/2003GL016946

Denton, R. E., Menietti, J. D., Goldstein, J., Young, S. L., & Anderson, R. R. (2004). Electron density in the magnetosphere. *Journal of Geophysical Research*, *109*, A09215. https://doi.org/10.1029/2003JA010245

D'haeseleer, W. D., Hitchon, W. N. G., Callen, J. D., & Shohet, J. L. (1991). *Flux coordinates and magnetic field structure*. Berlin, Germany: Springer-Verlag.

Elkington, S. R. (2006). A review of ULF interactions with radiation belt electrons. In K. Takahashi, et al. (Eds.), *Magnetospheric ULF waves: Synthesis and new directions, Geophysical Monograph Series* (Vol. 169, pp. 177–193). San Diego, CA: Chapman Conference on Magnetospheric ULF Waves.

Elkington, S., Hudson, M., & Chan, A. (1999). Acceleration of relativistic electrons via drift-resonant interaction with toroidal-mode Pc5 ULF oscillations. *Geophysical Research Letters*, *26*(21), 3273–3276.

Fälthammar, C.-G. (1965). Effects of time-dependent electric fields on geomagnetically trapped radiation. *Journal of Geophysical Research*, *70*(11), 2503–2516. https://doi.org/10.1029/JZ070i011p02503

Gillis, E. J., Rijnbeck, R., Kling, R., Speiser, T. W., & Fritz, T. A. (1987). Do flux transfer events cause long-period micropulsations in the dayside magnetosphere. *Journal of Geophysical Research*, *92*, 5820–5926. https://doi.org/10.1029/JA092iA06p05820

Glassmeier, K.-H., Lester, M., Mier-Jedrzejowicz, W. A. C., Green, C. A., Rostoker, G., Orr, D., … Amata, E. (1984). Pc5 pulsations and their possible source mechanisms—A case study. *Journal of Geophysics Zeitschrift Geophysik*, *55*, 108–119.

Goldstein, J., & Sandel, B. R. (2005). The global pattern of evolution of plasmaspheric drainage plumes. In J. L. Burch, M. Schulz, & H. Spence (Eds.), *Inner magnetosphere interactions: New perspectives from imaging, Geophysical Monograph Series* (Vol. 159, 1 pp.). Washington, DC: American Geophysical Union.

Goldstein, J., Sandel, B. R., Forrester, W. T., Thomsen, M. F., & Hairston, M. R. (2005). Global plasmasphere evolution 22–23 April 2001. *Journal of Geophysical Research*, *110*, A12218. https://doi.org/10.1029/2005JA011282

Hasegawa, A., & Chen, L. (1974). Theory of magnetic pulsations. *Space Science Reviews*, *16*(3), 347–359.

Herrera, D., Maget, V. F., & Sicard-Piet, A. (2016). Characterizing magnetopause shadowing effects in the outer electron radiation belt during geomagnetic storms. *Journal of Geophysical Research: Space Physics*, *121*, 9517–9530. https://doi.org/10.1002/2016JA022825

Hwang, K.-J., & Sibeck, D. G. (2016). Role of low-frequency boundary waves in the dynamics of the dayside magnetopause and the inner magnetosphere. In Keiling, A., Lee, D.-H., & Nakariakov, V. (Eds.), *Low-frequency waves in space plasmas, Geophysical Monograph Series* (Vol. 216, pp. 213–239). Hoboken, NJ: John Wiley. https://doi.org/10.1002/9781119055006

Kabin, K., Rankin, R., Mann, I. R., Degeling, A. W., & Marchand, R. (2007). Polarization properties of standing shear Alfven waves in non-axisymmetric background magnetic fields. *Annales de Geophysique*, *25*(3), 815–822.

Kale, Z. C., Mann, I. R., Waters, C. L., Goldstein, J., Menk, F. W., & Ozeke, L. G. (2007). Ground magnetometer observation of a cross-phase reversal at a steep plasmapause. *Journal of Geophysical Research*, *112*, A10222. https://doi.org/10.1029/2007JA012367

Kale, Z. C., Mann, I. R., Waters, C. L., Vellante, M., Zhang, T. L., & Honary, F. (2009). Plasmaspheric dynamics resulting from the Hallowe'en 2003 geomagnetic storms. *Journal of Geophysical Research*, *114*, A08204. https://doi.org/10.1029/2009JA014194

Kepko, L., & Spence, H. E. (2003). Observations of discrete, global magnetospheric oscillations directly driven by solar wind density variations. *Journal of Geophysical Research*, *108*(A6), 1257. https://doi.org/10.1029/2002JA009676

Kessel, R., Mann, I., Fung, S., Milling, D., & O'Connell, N. (2004). Correlation of Pc5 wave power inside and outside the magnetosphere during high speed streams. *Annales de Geophysique*, *22*(2), 629–641.

Kim, K.-H., Cattell, C. A., Lee, D.-H., Takahashi, K., Yumoto, K., Shiokawa, K., … Andre, M. (2002). Magnetospheric responses to sudden and quasiperiodic solar wind variations. *Journal of Geophysical Research*, *107*(A11), 1406. https://doi.org/10.1029/2002JA009342

Lee, D.-H., & Lysak, R. L. (1991). Impulsive excitation of ULF waves in the three-dimensional dipole model: The initial results. *Journal of Geophysical Research*, *96*(A3), 3479–3486. https://doi.org/10.1029/90JA02349

Li, Z., Hudson, M., Patel, M., Wiltberger, M., Boyd, A., & Turner, D. (2017). ULF wave analysis and radial diffusion calculation using a global MHD model for the 17 March 2013 and 2015 storms. *Journal of Geophysical Research: Space Physics*, *122*, 7353–7363. https://doi.org/10.1002/2016JA023846

Lysak, R. L., Song, Y., Sciffer, M. D., & Waters, C. L. (2015). Propagation of Pi2 pulsations in a dipole model of the magnetosphere. *Journal of Geophysical Research: Space Physics*, *120*, 355–367. https://doi.org/10.1002/2014JA020625

Mann, I. R., & Ozeke, L. G. (2016). How quickly, how deeply, and how strongly can dynamical outer boundary conditions impact Van Allen radiation belt morphology? *Journal of Geophysical Research: Space Physics*, *121*, 5553–5558. https://doi.org/10.1002/2016JA022647

Mills, K., Wright, A., & Mann, I. (1999). Kelvin-Helmholtz driven modes of the magnetosphere. *Physics of Plasmas*, *6*(10), 4070–4087.

Nunn, D. (1993). A novel technique for the numerical simulation of hot collision-free plasma; Vlasov hybrid simulation. *Journal of Computational Physics*, *108*, 180–196.

O'Brien, T., McPherron, R., Sornette, D., Reeves, G., Friedel, R., & Singer, H. (2001). Which magnetic storms produce relativistic electrons at geosynchronous orbit? *Journal of Geophysical Research*, *106*(A8), 15,533–15,544. https://doi.org/10.1029/2001JA000052

Piersanti, M., Villante, U., Waters, C., & Coco, I. (2012). The 8 June 2000 ULF wave activity: A case study. *Journal of Geophysical Research*, *117*, A02204. https://doi.org/10.1029/2011JA016857

Rae, I. J., Donovan, E. F., Mann, I. R., Fenrich, F. R., Watt, C. E. J., Milling, D. K., … Balogh, A. (2005). Evolution and characteristics of global Pc5 ULF waves during a high solar wind speed interval. *Journal of Geophysical Research*, *110*, A12211. https://doi.org/10.1029/2005JA011007

Rankin, R., Kabin, K., & Marchand, R. (2006). Alfvenic field line resonances in arbitrary magnetic field topology. *Advances in Space Research*, *38*(8), 1720–1729. https://doi.org/10.1016/j.asr.2005.09.034

Roederer, J. G. (1970). *Dynamics of geomagnetically trapped radiation*. New York: Springer.

Russell, C. T., & Elphic, R. C. (1978). Initial ISEE magnetometer results: Magnetopause observations. *Space Science Reviews*, *22*(6), 681–715. https://doi.org/10.1007/BF00212619

Samson, J. C., Jacobs, J. A., & Rostoker, G. (1971). Latitude-dependent characteristics of long-period geomagnetic micropulsations. *Journal of Geophysical Research*, *76*, 3675–3683.

Sandel, B., Goldstein, J., Gallagher, D., & Spasojevic, M. (2003). Extreme ultraviolet imager observations of the structure and dynamics of the plasmasphere. *Space Science Reviews*, *109*(1–4), 25–46. https://doi.org/10.1023/B:SPAC.0000007511.47727.5b, pT: J; UT: WOS:000187133000003.

Scholer, M. (1970). On the motion of artificial ion clouds in the magnetosphere. *Planetary and Space Science*, *18*, 977–1004. https://doi.org/10.1016/0032-0633(70)90101-7

Shprits, Y. Y., Elkington, S. R., Meredith, N. P., & Subbotin, D. A. (2008). Review of modeling of losses and sources of relativistic electrons in the outer radiation belt I: Radial transport. *Journal of Atmospheric and Solar-Terrestrial Physics*, *70*(14, Sp. Iss. SI), 1679–1693. https://doi.org/10.1016/j.jastp.2008.06.008, AGU Fall Meeting 2006, San Francisco, CA, December 11-15, 2006.

Singer, H. J., Southwood, D. J., Walker, R. J., & Kivelson, M. G. (1981). Alfven wave resonances in a realistic magnetospheric magnetic field geometry. *Journal of Geophysical Research*, *86*(A6), 4589–4596. https://doi.org/10.1029/JA086iA06p04589

Stern, D. (1975). The motion of a proton in the equatorial magnetosphere. *Journal of Geophysical Research*, *80*, 595–599.

Stern, D. P. (1985). Parabolic harmonics in magnetospheric modeling: The main dipole and the ring current. *Journal of Geophysical Research*, *90*(A11), 851–863.

Tan, L. C., Shao, X., Sharma, A. S., & Fung, S. F. (2011). Relativistic electron acceleration by compressional-mode ULF waves: Evidence from correlated Cluster, Los Alamos National Laboratory spacecraft, and ground-based magnetometer measurements. *Journal of Geophysical Research*, *116*, A07226. https://doi.org/10.1029/2010JA016226

Turner, D. L., Shprits, Y., Hartinger, M., & Angelopoulos, V. (2012). Explaining sudden losses of outer radiation belt electrons during geomagnetic storms. *Nature Physics*, *8*(3), 208–212. https://doi.org/10.1038/NPHYS2185

Vellante, M., Piersanti, M., Heilig, B., Reda, J., & Corpo, A. D. (2014). Magnetospheric plasma density inferred from field line resonances: Effects of using different magnetic field models. In *XXXIth URSI General Assembly and Scientific Symposium (URSI GASS)* (pp. 1–4). Beijing, China. https://doi.org/10.1109/URSIGASS.2014.6929941

Vellante, M., Piersanti, M., & Pietropaolo, E. (2014). Comparison of equatorial plasma mass densities deduced from field line resonances observed at ground for dipole and IGRF models. *Journal of Geophysical Research: Space Physics*, *119*, 2623–2633. https://doi.org/10.1002/2013JA019568

Volland, H. (1973). A semi-empirical model of large-scale magnetospheric electric fields. *Journal of Geophysical Research*, *78*, 171.

Walker, A. D. M. (1981). The Kelvin-Helmholtz instability in the low-latitude boundary-layer. *Planetary and Space Science*, *29*(10), 1119–1133.

Walker, A. D. M. (2000). Coupling between waveguide modes and field line resonances. *Journal of Atmospheric and Solar-Terrestrial Physics*, *62*, 799–813.

Waters, C. L., Sciffer, M. D., & Lysak, R. L. (2010). FDTD modeling of ULF waves in the magnetosphere and ionosphere. In *2010 International Conference on Electromagnetics in Advanced Applications* (pp. 477–480). Sydney, NSW, Australia. https://doi.org/10.1109/ICEAA.2010.5653758

Zong, Q.-G., Zhou, X.-Z., Wang, Y. F., Li, X., Song, P., Baker, D. N., … Pedersen, A. (2009). Energetic electron response to ULF waves induced by interplanetary shocks in the outer radiation belt. *Journal of Geophysical Research*, *114*, A10204. https://doi.org/10.1029/2009JA014393